HHS Public Access

Author manuscript

NanoImpact. Author manuscript; available in PMC 2021 April 01.

Published in final edited form as:

NanoImpact. 2020 April ; 18: . doi:10.1016/j.impact.2020.100215.

Comparison of *in vitro* toxicity of aerosolized engineered nanomaterials using air-liquid interface mono-culture and co-culture models

Yifang Wang[a], **Andrea Adamcakova-Dodd**[b], **Benjamin R. Steines**[b], **Xuefang Jing**[b], **Aliasger K. Salem**[c], **Peter S. Thorne**[a,b,*]

[a]Human Toxicology Interdisciplinary Program, University of Iowa, Iowa City, IA, USA

[b]Occupational and Environmental Health, University of Iowa, Iowa City, IA, USA

[c]College of Pharmacy, University of Iowa, Iowa City, IA, USA

Abstract

Airborne engineered nanomaterials (ENMs) can readily enter the human body through inhalation potentially leading to adverse health effects such as cardiovascular and pulmonary diseases. Our group has previously utilized and validated an integrated low flow system capable of generating and depositing airborne ENMs directly onto cells at an air-liquid interface (ALI). To further improve this ALI method for an even closer representation of the *in vivo* system, a co-culture model containing epithelial, endothelial and macrophage cell lines (A549, EA.hy 926, and THP-1 differentiated macrophages) was established and validated for testing ENMs toxicity. In the co-culture model, cells were exposed to citrate-capped gold (Au), 15% silver on silica (Ag-SiO_2) and copper oxide (CuO) ENMs under the same protocol (4 h ALI exposure with a target concentration of 3.5 mg/m^3) and compared to responses with A549 cells only or THP-1 differentiated cells only. The toxicological profile was assessed by measuring cell viability, reactive oxygen species (ROS) production, lactate dehydrogenase (LDH) release, and interleukin (IL)-8 concentration. Results showed that 15% Ag-SiO_2 induced more oxidative stress-related toxicity in the co-culture than in A549 cells alone. Both 15% Ag-SiO_2 and CuO exposure produced significantly higher levels of IL-8 in the co-culture compared with A549 cells alone. Citrate-capped Au was largely inert. Further exposures of CuO on macrophages alone provided evidence of cell-cell interaction in the co-culture model. In addition, the co-culture model exhibited a similar response to primary human bronchial epithelial cells in terms of ROS and IL-8 responses after CuO exposure, suggesting a more advanced refinement of the conventional model for *in vitro* inhalation study.

*Corresponding authors at: Department of Occupational and Environmental Health, The University of Iowa, College of Public Health, 145 N. Riverside Dr., S341A CPHB, Iowa City, IA 52242, USA. peter-thorne@uiowa.edu (P.S. Thorne).

CRediT authorship contribution statement

Yifang Wang: Methodology, Formal analysis, Investigation, Writing - original draft.**Andrea Adamcakova-Dodd:**Conceptualization, Methodology, Formal analysis, Writing - review & editing, Funding acquisition.**Benjamin R. Steines:**Methodology, Investigation.**Xuefang Jing:**Methodology, Investigation.**Aliasger K. Salem:**Conceptualization, Funding acquisition.**Peter S. Thorne:**Conceptualization, Methodology, Formal analysis, Writing - original draft, Writing - review & editing, Supervision, Project administration, Funding acquisition.

Declaration of competing interest

The authors declare that they have no known competing financial interests or personal relationships that could have appeared to influence the work reported in this paper.

Keywords

Nanoparticles; *In vitro* toxicology; Air interfaced culture; Air-liquid interface; Co-culture; A549; THP-1; EA.hy 926

1. Introduction

The application and production of ENMs has increased dramatically in the last decade. These newly developed materials are used in over 1600 consumer products today. With diverse chemical compositions, shapes, sizes and chemical properties these materials are designed to fit specific functions. For example, silver ENMs are used in toothpastes for their antibacterial property, titanium dioxide or zinc oxide ENMs are added to sunscreens because they effectively block ultraviolent light, and carbon nanotubes are manufactured for electronics, optics, and many other uses (Kessler, 2011). During the process of production, workers have the potential to inhale elevated concentrations of ENMs. Unfortunately, safety assessments of these new ENMs lag behind their use in manufacturing and commerce. Higher throughput toxicity assessment methods are needed for more rapid screening of these ENMs. Conventional submerged cell culture conditions have been used for screening ENMs; however, recognized limitations include unrealistic exposure conditions and inconsistent biological responses compared with *in vivo* models. Therefore, we evaluated an advanced *in vitro* air-liquid interface (ALI) method to study biological responses in a three-cell system with various ENMs including citrate-capped gold (Au), 15% silver supported on silica (Ag-SiO_2), and copper oxide (CuO).

Spherical Au ENMs have many unique physicochemical properties including fluorescence quenching, redox activities, and surface plasmons (electron oscillations). Therefore, Au ENMs have been widely used for biomedical imaging and sensing and therapeutics (Yeh et al., 2012). Published studies regarding the toxicity of Au ENMs have drawn distinct and even contrary conclusions. One study found no toxicity of 15 nm Au ENMs in a human primary co-culture model while another study found that 25 nm Au ENMs induced pro-inflammatory responses in epithelial cells (Rothen-Rutishauser et al., 2007; Brandenberger et al., 2010). The difference may have been due to different experimental designs or differing properties of the Au ENMs.

Ag-SiO_2 ENMs are of interest to the scientific community due to their stable catalytic properties and their wide use in industry. SiO_2 which provides stability supporting the silver ENMs without altering the catalytic activity (Ramnani et al., 2007; Jiang et al., 2005). Recently, toxicology studies for silver ENMs have shown cytotoxicity, ROS production and reduction of cell viability in human-derived cell lines as well as a permeability increase in rat liver mitochondria (AshaRani et al., 2009; Hussain et al., 2005; Almofti et al., 2003). The toxicity of silica ENMs is relatively complex because of different shapes, method of synthesis and exposure routes, but studies have generally found they are toxic (Murugadoss et al., 2017). Toxicological data regarding Ag-SiO_2 ENMs remains scarce.

CuO ENMs are also commonly used in industry for sensors, catalysts, semiconductors, and in cosmetics for their chemical reactivity and antimicrobial properties (Katwal et al., 2015;

Grigore et al., 2016). CuO ENMs induce toxicity in human lung epithelial cells lines including significant cell death, ROS production, excessive cytokine releases, and DNA damage (Jing et al., 2015; Karlsson et al., 2008). In addition, exposure of CuO ENMs to mice by nasal instillation demonstrated epithelial cell injury, pulmonary inflammation and lung fibrosis in a dose-dependent manner (Lai et al., 2018). In our study, CuO was included as a known positive for toxicity and served to validate the method and act as a comparator for other nanomaterials.

To evaluate the toxicity of ENMs supplied through the Nanotechnology Health Implications Research (NHIR) Consortium, we applied a co-culture model utilizing human lung alveolar adenocarcinoma epithelial cells (A549), human differentiated monocytes (THP-1), and human umbilical vein endothelial cells (EA.hy 926). EA.hy 926 is a well-characterized endothelial cell line that is a hybridization of A549 cells and the HUVEC human primary endothelial cell line. The hybridization gives EA.hy 926 cells a high stability in biological assays but also preserves most characteristics of primary endothelial cells (Edgell et al., 1983; Bouis et al., 2001). In addition, previous data have shown the legitimacy of using EA.hy 926 cells in respiratory co-culture models (Klein et al., 2013). The goal of these studies was to establish and validate this co-culture model, use this system for ENM toxicity testing, and compare the results with monoculture models. Our hypothesis was that the complexity of the co-culture model would show enhanced biological responses over the monoculture system using the same ENMs.

2. Materials and methods

2.1. In vitro ALI exposure system

Our *in vitro* exposure system has been previously described (Kim et al., 2013). Briefly, the system is composed of an ENM generation system, a Scanning Mobility Particle Sizer (SMPS), and the Vitrocell exposure device (Vitrocell Systems, GMBH, Waldkirch, Germany) [Fig. 1]. ENM suspensions were aerosolized using a 6-jet Collison nebulizer (CH Technologies, USA). The Collison nebulizer was operated at an air pressure of 103 kPa (15 psi) for the 15% Ag-SiO_2, CuO and low concentration Au. The pressure was increased to 124 kPa (18 psi) and the dilution air flow was reduced to generate the higher Au concentration with the same airflow delivered to the aerosol distribution system. ENM aerosol flowed through a moisture removal system consisting of a 30-cm long 110 °C brass column and a vapor condenser. The dried aerosol then passed through a charge neutralizer (Soft X-ray Neutralizer, model 3088, TSI Inc., Shoreview, MN) to remove electrostatic charges prior to entering the ALI exposure chamber and the SMPS (model 3080 Electrostatic Classifier with model 3081 Differential Mobility Analyzer and model 3785 Condensation Particle Counter, TSI Inc., Shoreview, MN). In the ALI exposure system, up to six transwells were placed into direct contact with incoming aerosol. Cell culture medium was supplied at the basal side (16 mL per each chamber with transwell). The exposure system was maintained at 37 ± 0.1 °C using a circulating water bath. The total flow rate entering the ALI cell chamber was 4.75 L/min of air supplemented with 0.25 L/min of CO_2 to yield 5% CO_2, optimal for lung cells. Each transwell received 0.1% of the total flow (5

mL/min) through separate aerosol inlets maintained by mass flow controllers (GFC17, Aalborg Instruments, Orangeburg, NY, USA).

2.2. ENMs sources and characterizations

The NHIR Engineered-nanomaterials Resource Coordination Core (ERCC) at the Harvard School of Public Health provided all ENMs used in this study [Table 1]. Prior to exposure, 0.5 mg/mL of 15% Ag-SiO_2 or 1.5 mg/mL of CuO ENM powder [Table 2] was suspended in Optima LC/MS grade water (Fisher Scientific, Pittsburgh, PA). The suspension was sonicated (3 min) using a cup horn sonicator (QSonica, CT) and then vortexed sequentially three times. The concentrations of the ENMs suspension in the nebulizer were decided experimentally to yield an airborne concentration of 3.5 mg/m^3. The sonication amplitude and time was specific for different ENMs. Exposure concentrations of generated ENM aerosols ranged from 2.48 to 4.73 mg/m^3 [Table 2]. Citrate-capped Au nanoaerosol was generated in two exposure concentrations: low (1.58 mg/m^3) and high (2.48 mg/m^3). Deposited doses per unit surface area, D_A, of each the culture well were calculated [Table 3] using following equation:

$$D_A = \frac{C \cdot Q_{transwell} \cdot T \cdot \alpha_{vitrocell}}{A_{transwell} \cdot 10^{6ml/m^3}},$$

where D_A has the units of ng/cm^2 and C is the ENM concentration of generated aerosol (ng/m^3); $Q_{transwell}$ is the flow rate to each individual transwell (5 mL/min); T is exposure time (min); $\alpha_{vitrocell}$ is the estimated deposition fraction in the Vitrocell system (50%); $A_{transwell}$ is the cell growth area on transwell of 6-well plate (4.67 cm^2).

2.3. Cell culture

Human lung carcinoma alveolar epithelial cells (A549) were purchased from ATCC (American Type Culture Collection, #CCL-185, Manassas, VA, USA). A549 cells were cultivated in Dulbecco's Modified Eagle Medium (with 4.5 g/L glucose, 4 mM L-glutamine, Hyclone Laboratories, Inc., Logan, UT, USA) and supplemented with 10% fetal bovine serum (FBS, Hyclone Laboratories) and 1% penicillin (100 units/mL) and streptomycin (100 μg/mL, Invitrogen, Carlsbad, USA) at 37 °C in a humidified atmosphere containing 5% CO_2. For ALI exposure, cells were harvested with 0.25% trypsin-ethylenediamine tetraacetic acid without phenol red (Trypsin-EDTA, Invitrogen), counted and seeded onto 4.7 cm^2 transwell membranes without collagen treatment (No. 3450, polyester, 0.4 μm, Transwell, Corning, NY, USA). A549 cell doubling time across experiments was 22–28 h. When cells grew confluent, the apical medium was removed and cells were cultured at an ALI for 12 h prior to exposure. Cells were washed twice with Dulbecco's Phosphate Buffer Saline (DPBS) and then transferred to the *in vitro* exposure system where they were supplied with RPMI 1640 medium (phenol red-free) from the basal side through the semipermeable transwell membrane. The exposure period was selected to be 4 h, based on our earlier evaluation for ALI. (Jing et al., 2015; Kim et al., 2013) A constant pH was maintained by using medium buffered with 25 mM hydroxyethyl piperazine ethanesulfonic acid (HEPES, Invitrogen).

EA.hy 926 and THP-1 cells were purchased from ATCC (#CCL-185) and authenticated as described below. EA.hy 926 cells were cultivated in Dulbecco's Modified Eagle Medium (with 4.5 g/L glucose, 4 mM L-glutamine) and supplemented with 10% FBS and 1% penicillin (100 units/mL) and streptomycin (100 μg/mL). EA.hy 926 cells demonstrated a doubling time of 12–16 h. In addition, THP-1 cells were grown in RPMI 1640 medium (with L-glutamine and 25 mM HEPES, Corning, 10–041-CV) and supplemented with 10% FBS, 1% penicillin (100 units/mL) and streptomycin (100 μg/mL), 1% sodium pyruvate (Gibco, 11360070), 1% GlutaMAX (Gibco, 35050061), and 0.05 mM 2-Mercaptoethanol (VWR, 97064588). THP-1 cells had a longer doubling time of 36–40 h. Cell lines were cultivated at 37 °C in a humidified atmosphere containing 5% CO_2.

To build the co-culture system, THP-1 cells were differentiated into macrophages by treatment with 200 nM phorbol 12-myristate 13-acetate (PMA) (Sigma-Aldrich, P1585) for 48 h, washed and rested for another 48 h. Cells were harvested, counted and applied to the transwells at specific seeding densities as follows: A549 cells: 5.32×10^4 cells/cm^2; THP-1 cells: 2.13×10^4 cells/cm^2; and EA.hy 926: 4.25×10^4 cells/cm^2. EA.hy 926 cells were seeded on the inverted transwell plates and incubated at the optimal cell culture condition for about 2 h until attached. The transwells were flipped after attachment, and 2 mL of medium were added to the basal side of the transwells. The plate was returned to the incubator. The next day, A549 cells were counted and seeded on the apical side of the transwells. On the third day, differentiated THP-1 cells were counted and seeded on top of the A549 cells. The epithelial and endothelial cells were allowed to grow to confluence.

Medium on the apical side of the transwells was removed 12 h before exposure for the epithelial cells and macrophages to adapt to the ALI condition. Briefly, the co-culture of cells was exposed to the same concentrations of ENMs as previously described under ALI for 4 h. During exposure, particle size distribution of generated nanoaerosol was measured every hour. Immediately after 4 h exposure, the co-culture cells were washed with DPBS for detection of cytokines and LDH. The washes were centrifuged at 14,000*g* for 15 min at 4 °C to remove ENMs and were frozen at −80 °C. Next, cells were removed from the transwells for cell viability and ROS assays.

2.3.1. Transepithelial electrical resistance (TEER) measurement—TEER values were measured daily for A549 cells, EA.hy 926 cells, and the co-culture system from day 1 to day 13 by Epithelial Volt/Ohm Meter (EVOM2, WPI, LLC Sarasota, FL USA) as shown in Fig. S1. Briefly, each group was prepared in triplicate, and each well was measured thrice. A group of medium only was used as the negative control. The TEER values were determined by the average value of each group minus the average of the medium-only group. TEER values were multiplied by the surface area of the inserts (4.2 cm^2).

2.3.2. Cell barrier integrity—Tight junction paracellular permeability was measured using sodium fluorescein salt (F6377, Sigma-Aldrich) dissolved in ultra-pure water with a concentration of 10 μg/mL. A triplicate of A549 cells only, EA.hy 926 cells only, co-culture system and no-cell controls were measured as replicates on day 9. The fluorescein solution was added to the apical side of transwells, and the plate was incubated at 37 °C in a humidified atmosphere containing 5% CO_2 in the dark for 1 h. After incubation, medium

from the basal side was transferred to a 96-well cell culture plate. The fluorescence readouts were measured using a microplate reader (SpectraMax M5, Molecular Devices LLC, USA) with an excitation wavelength 460 nm and an emission wavelength 515 nm.

2.3.3. TEM imaging—Co-culture model cells were fixed overnight at 4 °C with 2.5% glutaraldehyde. The cells were then stained with 1% osmium tetroxide with 1.5% potassium ferrocyanide, and 2.5% uranyl acetate. Next, a graduated increase in acetone concentration was used to dehydrate the sample prior to embedding at 70 °C overnight. The samples were microtomed, uranyl and lead stained, and examined using TEM (JEOL JEM-1230 TEM, JEOL, USA). Image acquisition was performed by the Gatan UltraScan 1000 2 k × 2 k CCD digital imaging system (Gatan, Inc. USA).

2.3.4. Multicolor immunofluorescent (IF) staining—Cells were placed on ice for 5 min before fixation, then were washed in cold DPBS and fixed with 4% formaldehyde in DPBS at 22 °C for 15 min. Fixed cells were washed thrice with DPBS to remove any residual formaldehyde. The co-culture cell lines were further treated with 0.5% Triton X-100 in DPBS for 10 min at 22 °C to increase their permeability. Cells were again washed and treated for 50 min with blocking buffer (Superblock 37515, Thermo Fisher Scientific, USA). Next cells were incubated with appropriate primary and secondary antibodies in a 37 °C-humidified shaker for 1 h in the dark. To avoid cross-reaction of antibodies and antigens, antibodies were added sequentially to the apical and basal compartments of the filter membranes. ZO-1 rabbit polyclonal primary antibody (1:100 dilution, 61–7300, Thermo Fisher Scientific) was added to the apical side to stain A549 tight junction protein. Next mouse anti-human von Willebrand factor (VWF) primary antibody (1:50 dilution, sc-365712, Santa Cruz Biotechnology) was added to the basal side for recognizing EA.hy 926 cells. Mouse anti-human CD68 (KP-1) Alexa Fluor 488-conjugated antibody (1:100 dilution) (sc-20060, Santa Cruz Biotechnology, USA) was used to detect THP-1 differentiated macrophages in the final step. Secondary antibodies were as follows: goat anti-rabbit ZO-1 secondary antibody Alexa Fluor 633 1:500 (A-21071, Thermo Fisher Scientific, USA), goat anti-mouse VWF secondary antibody Alexa Fluor 555 1:500 (A-21422, Thermo Fisher Scientific, USA). The nuclei were counter-stained using 4′, 6′-diamidino-2-phenylindole (DAPI) for 1 min before the last wash (62247, Thermo Fisher Scientific, USA). The filters were cut from the microplates and mounted on glass slides in mounting gel. A Zeiss LSM 710 upright confocal microscope (Carl Zeiss Microscopy, Germany) was used to analyze samples with images capture by Zen imaging software 2009 (Carl Zeiss Microscopy).

2.4. Measures of toxicity

2.4.1. Cell viability—Immediately after 4 h exposure, cells were detached from the transwells with 0.25% Trypsin-EDTA (Gibco). Cell viability was assessed using the MoxiCyte Viability Kit (#MXA055, Orflo Tech, LLC, Ketchum, ID). The general cell membrane integrity was assessed by dye-exclusion, measured by propidium iodide (PI) staining (561 nm) and quantified using cytometry (MXG102, Moxi GO II, Orflo Technologies). Briefly, detached cells were counted and prepared in a concentration range of 1×10^5 to 3×10^6 cells/mL to fit the optimal detection range of the instrument. Cell

suspension was diluted 10× using PI solution. The mixture was incubated in the dark for 5 min at room temperature. A positive control (cells exposed to 80 °C for 20 min) and a negative control (fresh cells taken from the incubator) were prepared for instrument gating.

2.4.2. Oxidative stress—Intracellular oxidative stress was measured using dithydroethidium (DHE), which is a widely used redox sensitive fluorescent probe (Item # 601290, Cayman, Ann Arbor, MI, USA). DHE is oxidized by superoxide to form 2-hydroxyethidium (excitation 500–530 nm/emission 590–620 nm) or by non-specific oxidation from other sources of ROS to form ethidium (excitation 480 nm/emission 576 nm) (Dikalov and Harrison, 2014). Each time the assay was performed a positive control treated with 300 μM Antimycin A to induce ROS, and a negative control using 300 mM antioxidant *N*-acetyl cysteine treated with DHE solution were used. A maximum 1×10^5 cells were prepared for each sample. Cells were centrifuged, washed with buffer, and incubated with 1:500 diluted DHE solution in the dark. After incubation, the cell suspension was transferred to a black, flat bottom 96-well plate. Fluorescence emission was measured using a microplate reader (SpectraMax M5, Molecular Devices) with 485 nm excitation and 590 nm emission.

2.4.3. Cytotoxicity—Cellular cytotoxicity was assessed by the level of lactate dehydrogenase (LDH) activity. Damaged cells release cytoplasmic LDH enzyme which converts lactate to pyruvate *via* reduction of NAD^+ to NADH. After ENM exposure, A549 cells were washed with DPBS buffer and washes were centrifuged at 12,000*g* and stored at −80 °C. LDH was detected using a Cytotoxicity Detection Kit (Roche Diagnostics, Mannheim, Germany). The absorbance was measured at 490 nm using a microplate reader (SpectraMax M5) with a reference wavelength above 600 nm. An L-LDH standard (Roche) in serial dilutions was used to calculate the LDH activity in cell wash solutions.

2.4.4. Inflammatory responses—Before cells were detached from the transwell, they were washed with 800 μl DPBS. Cell washes were centrifuged at 14,000 ×*g* for 30 min and stored at −80 °C for cytotoxicity and cytokine assays. Inflammatory responses after ENMs exposure were determined by quantifying the amount of IL-8 released using the human IL-8 ultrasensitive ELISA kit (Cat.KHC0084, Life Tech, USA) with a standard curve covering the range of 0.39–25 pg/mL.

2.5. Statistical analyses

All data were analyzed using Student's *t*-test (Sigma Plot v.11.0, Systat Software Inc., Point Richmond, CA). Statistical probability (P values) in plots are expressed as follows: *** $P < 0.001$, ** $P < 0.01$, and * $P < 0.05$. Data for cell viability, production of ROS, release of LDH and IL-8 concentration were normalized to each corresponding incubator control (control) and are expressed in plots as percentage of control. Data are expressed as mean ± standard deviation (SD) unless otherwise noted.

3. Results

3.1. Characterization of ENM aerosol

Citrate-capped Au, 15% Ag-SiO_2, and CuO ENMs were supplied and characterized by the ERCC (Zimmerman et al., 2019; Beltran-Huarac et al., 2018; Dong et al., 2020; Eweje et al., 2019). Table 1 presents ENM characterization data including size, shape, crystal structure, density, purity and endotoxin concentration. All ENMs had a primary particle size 50 nm in diameter of less as determined by TEM [Table 2]. The smallest primary particle size was measured for 15% Ag-SiO_2 (8 nm) and the largest was CuO (50 nm). The geometric mean mobility diameter of generated aerosol for all ENMs studied was between 35 and 76 nm. Thus, minimal aggregation/agglomeration was observed. As shown in Fig. 2, both Au citrate-capped and CuO ENMs showed unimodal particle size distributions. For 15% Ag-SiO_2, the distribution was more indicative of overlapping bimodality with peaks at 50 nm and 100 nm. ENM particle counts for different cell culture experiments ranged from 0.68–3.0 × 10^6 particles/cm^3 [Table 2]. Estimated deposited doses per surface area of the well for high dose of citrate-capped Au, 15% Ag-SiO_2 and CuO ENMs are provided in Table 3 and ranged from 203 to 608 ng/cm^2. The supplied ENM were assayed for endotoxin activity and found to have a low degree of contamination [Table 1]. Nominal endotoxin loading values ranged from 0.0010 to 0.0016 EU/cm^2 for Au and CuO. The value for Ag-SiO_2 were higher at 0.014 to 0.015 EU/cm^2 [Table 3]. Chuang and colleagues reported that 12 h endotoxin exposure of A549 cells in T75 flasks at concentrations of 1.0 μg/mL, corresponding to approximately 2700 EU/cm^2, did not influence cell viability, induce apoptosis, effect biosynthesis of nitric oxide, nor alter the mitochondrial membrane potential (Chuang et al., 2011). Thus, these levels of endotoxin are below levels associated with pro-inflammatory activity.

3.2. Verifying establishment of co-culture and cell barrier integrity

TEER was measured from day 1 after establishment of individual cell cultures and the co-culture to day 13 every 24 h in triplicate [Fig. 3A]. From day 1 to day 6, all four cultures increased their resistance. From day 4 to day 13, A549 and EA.hy 926 cultures tracked one another closely. From day 1 to day 13 the TEER value of the co-culture remained above those of the three mono-cultures and was significantly greater during the window for ENM exposures, days 6 to 9 ($P < 0.001$). TEER fell dramatically from day 9 to day 11. Tight junction paracellular permeability was evaluated as another measure of barrier integrity. As shown in Fig. 3B, co-cultures showed significantly reduced leakage of the tracer from the apical side to the basal side of the transwell compared with EA.hy 926 cell alone.

The architecture of the co-culture model was confirmed under TEM. Three cell layers were observed: epithelial cells [Fig. 4A, a] and endothelial cells [Fig. 4A, b], were observed on each side of the transwell membrane; EA.hy 926 cells are flatter than A549 cells [Fig. 4A]. In addition, two layers with distinct morphologies were detected on the apical side as demonstrated in Fig. 4B where macrophages are shown resting on the A549 cell layer.

Immunofluorescent staining was performed to verify each cell line in the co-culture model. The tight junction protein of A549 cells was recognized by ZO-1 expression [Fig. 5A]. ZO-1

staining showed an obvious honeycomb structure. Nuclei were counter-stained by DAPI in blue. CD68 for THP-1 differentiated macrophages was visualized in green [Fig. 5B]. In addition, the endothelial cell layer was only detected at the basal side of the transwells [Fig. 5C]. An immunofluorescence scanning confocal video illustrates the three-dimensional structure of the co-culture model [see Supplement Video].

3.3. Measures of toxicity

3.3.1. Cell viability—Citrate-capped Au did not significantly reduce the viability of A549 cells at either low or high concentration compared to incubator controls or filtered-air exposed cells. However, 15% Ag-SiO_2 induced a 25% loss of cell viability, and CuO induced a 30% decrease in viability compared with controls [Fig. 6A]. There was a further decrease in cell viability in the co-culture model after treatment with 15% Ag-SiO_2 compared to A549 cell alone [Fig. 7A]. The decrease of viability in both models after CuO ENM exposure was similar.

3.3.2. Oxidative stress—ROS production was measured using dihydroethidium (DHE) which produces fluorescence when oxidized by superoxide and hydrogen peroxide. Exposure to filtered air and Au ENMs induced minimal ROS in both high and low exposure concentrations. However, we observed about 1.7-fold increase in ROS after 15% Ag-SiO_2 exposure, and a 2-fold increase after CuO exposure of A549 cells [Fig. 6B]. ROS production in the co-culture model was over twice as high as in the monoculture model ($P < 0.01$) after exposure to 15% Ag-SiO_2 [Fig. 7B]. CuO exposure increased ROS 2.4-fold over controls in the co-cultures compared with a 2.1-fold increase in the monoculture over controls.

3.3.3. Cytotoxicity (LDH)—Lactate dehydrogenase (LDH) served as a biomarker for damage to cell membrane integrity. For the monoculture studies, the LDH concentrations were very close between filtered air and incubator control groups as was observed for viability and ROS results. High dose citrate-capped Au ENMs elicited a small but significant LDH release ($P < 0.05$) compared to controls, but the LDH concentration after exposure to low dose Au ENMs was not different from controls [Fig. 6C]. However, both 15% Ag-SiO_2 and CuO had significant amounts of LDH release: about 7-fold higher for 15% Ag-SiO_2 and over 8-fold higher for CuO [Fig. 6C]. As illustrated in Fig. 7C, cells in the co-culture model followed the same trend as for the monoculture but with even higher amounts of LDH release.

3.3.4. Pro-inflammatory response (IL-8)—IL-8 was employed as a marker of inflammation. Consistent with ROS and LDH production in A549 cells, the filtered air and Au ENMs at the low concentration induced an insignificant increase of IL-8. However, we observed a significant increase in IL-8 production for the high dose Au exposure. 15% Ag-SiO_2 induced a 3-fold higher IL-8 concentration, and CuO induced a 6-fold increase compared with controls [Fig. 6D]. Fig. 7D demonstrates the difference of IL-8 level for monoculture *vs.* co-culture after exposures. We observed 6-fold and 29-fold increases after treatment with 15% Ag-SiO_2 and CuO ENMs, respectively compared with incubator controls. The difference between co-culture and monoculture was also statistically significant for 15% Ag-SiO_2 ($P < 0.01$) and for CuO ($P < 0.001$).

3.4. Toxicological responses of THP-1 differentiated macrophages after CuO ENMs exposure

THP-1 differentiated macrophages when exposed alone to CuO ENMs exhibited lower toxicity compared to the A549 cells and the co-culture model - the reduction in cell viability was only about 7% from controls [Fig. 8A]. This may be attributable to lower susceptibility of THP-1 cells and the lower exposure concentration delivered to the THP-1 cells as compared to the A549 cells or co-cultures. LDH release was marginally higher for CuO-exposed THP-1 cells compared to unexposed cells [Fig. 8C]. However, both ROS and IL-8 production were significantly elevated in the CuO exposed *vs.* controls [Fig. 8B and D]. Importantly, IL-8 concentration was increased 4-fold over controls for THP-1 cells alone *versus* an increase of 29-fold seen for the co-culture cells exposed to CuO [Fig. 7D].

4. Discussion

A functional human respiratory system involves many components, including epithelial cells, mucociliary system, airway immune cells as well as countless complex mechanistic pathways for protection against environmental toxicants. For decades, animal models have been used in toxicology research due to their robust representation of human toxic effects. However, there has been a push for development of alternative methods that reduce animal use (Gibb, 2008). We previously demonstrated an *in vitro* monoculture ALI model to investigate the toxicity of various ENMs (Jing et al., 2015; Kim et al., 2013). However, a limitation of the monoculture systems is that they lack cell-cell interactions that may be important for the development or mitigation of toxicity (Kim et al., 2013). To combat this limitation, we applied a co-culture model using three cell types to the study ENM toxicity. We were guided by several prior studies that established other co-culture models using various cell lines (Hermanns et al., 2004) and primary cells (Rothen-Rutishauser et al., 2005; Yonker et al., 2017).

Our group has previously documented the toxicity of CuO ENMs using a murine inhalation model and an *in vitro* ALI model. The toxicity of CuO ENMs was clearly demonstrated with increased recruitment of inflammatory cells to the lungs and increased LDH and cytokines/chemokines in bronchoalveolar lavage fluid, as well as cell viability loss (Jing et al., 2015; Kim et al., 2013; Pettibone et al., 2008). In the present study, A549 cells and co-cultures were exposed to Au, 15% Ag-SiO_2 and CuO ENMs under ALI condition for 4 h. We observed no toxicity for low dose Au, but moderate level irritation and inflammation when the exposure concentration of Au ENMs doubled suggesting modest, dose-dependent toxicity. However, we found greater toxicity for both 15% Ag-SiO_2 and CuO ENMs for all biological responses measured. CuO ENMs caused more damage in A549 cells than 15% Ag-SiO_2 ENMs at a lower delivered mass-based dose.

Silver is recognized to have antibacterial properties and has been employed as a disinfection agent and for treatment of burns, in part due to its low toxicity to human cells (Clement and Jarrett, 1994). However, 15% Ag-SiO_2 ENMs may undergo some dissolution to produce Ag (I) ions (Pradhan et al., 2016). Research on the localization of Ag (I) ions treated with bacteria showed that a large portion of Ag (I) ions were bound to cell membranes. The Ag (I) ions are reported to have a high affinity to surface and intracellular proteins and

polysaccharides and some reports indicate they inhibit oxidative enzymes (Russell and Hugo, 1994). Once they enter the cells, Ag cations were found to be associated with RNA and DNA fractions (Modak and Fox Jr., 1973). Consequently, the possible mechanism of toxicity was related to the prevalent membrane surface binding and disruption of normal membrane functions and DNA, RNA synthesis (Bickel, 1993). The other component of this material, SiO_2, occurs in distinct molecular structures, either crystalline or amorphous. Inhalation of crystalline silica in occupational settings is well known to cause silicosis (Society, 1997). On the other hand, less is known about the amorphous silica that formed the Ag-SiO_2 used in our studies. Studies reported contradictory results due to variations of exposure models, materials, and experimental protocols. Some reported that amorphous silica is less toxic than crystalline silica; however, others showed equal toxicity to mouse alveolar macrophages, but not mouse lung epithelial type II cells (Costantini et al., 2011). In our studies with Ag-SiO_2, the condition is more complex due to the likely exposure to both Ag (I) ions elemental Ag and amorphous SiO_2.

The toxicity of nanoscaled metallic copper and its oxides are well established. Wang et al. (Wang et al., 2012) demonstrated that CuO ENMs were taken up by A549 cells through endocytosis and induced DNA damage and ROS production in nuclei and mitochondria. Unoxidized metallic copper is a relatively unreactive metal. However, when Cu is exposed to air it is oxidized to Cu_2O and CuO (Pettibone et al., 2008). Moreover, as demonstrated by several studies, transition metals such as cadmium, zinc, copper, iron, chromium and titanium are able to release ions when they dissolve. These ions have the potential to react with local oxygen metabolic products to produce hydroxyl radicals and superoxide anions, and consequently lead to increased cytokine release, genotoxicity, and cell death (Cho et al., 2013; Nabeshi et al., 2011).

Interestingly, copper, silver and gold are three of the four ‘group 11 elements’ on the periodic table because each of them contains one sorbital on top of a filled electron shell that makes them share many similar chemistries for example, high electrical conductance, malleability, and antiseptic properties. In addition, due to their unique electron configurations, the reactivity decreases from Cu to Au creating a rank of Cu > Ag > Au, which also reflect the toxicity rank we observed. Our results confirm that chemical reactivity plays a major role in toxicological responses.

In vitro co-culture models have recently gained attention with research devoted to model construction and validation. There have been few toxicology studies with ENMs comparing co-culture and monoculture ALI systems. Our goal was to assess biological responses to ENM exposure in our co-culture model and compare the results with the monoculture model. We also sought to gain insight into the feasibility of using our ALI co-culture model in pulmonary toxicity studies.

The architecture of the co-culture model with endothelial cells on the basal side of the transwell and epithelial cells and macrophages on the apical side was inspired by the *in vivo* anatomy of the alveolar region. Once deposited on the surface of the lung epithelium, particles encounter alveolar macrophages, airway surface liquid and surfactant proteins. Nanoparticle clearance occurs by the mucociliary escalator, macrophage uptake and

transport through epithelial cells and across tight junctions (Kiama et al., 2001). These transportation mechanisms lead to translocation of particles into the interstitial space, lymphatic drainage and endothelial cells (Oberdorster et al., 2005a). A549 cells were selected for use because they mimic the morphological and biochemical properties of human pulmonary cells and secrete surfactant protein. Although A549 cells are a standard cell line in many *in vitro* pulmonary toxicology studies, they express an atypical tight junction that yields lower TEER values than primary human bronchial epithelial cells. Similarly, the human endothelial cell line, EA.hy 926, demonstrated TEER values 10-fold lower than human pulmonary microvascular endothelial cells (Srinivasan et al., 2015). This represents a limitation in using these cell lines. However, our results indicated significantly enhanced tight junction formation in our co-culture model over our monoculture model, somewhat mitigating this limitation.

In addition to TEER measurements, barrier integrity was assessed using a fluorescent tracer. Although both methods quantify the barrier integrity in the co-culture model, they have distinct features: TEER measurement focuses on the ionic conductance of the paracellular routes, while the permeability of the tracer is responsible for all of the non-electrolyte pathways such as fluid flows and the pore size of the tight junctions (Zucco et al., 2005). We observed the co-culture model had a lower permeability rate than single cell layers or the negative control, indicating an improved paracellular pathway integrity. Immunofluorescent staining also qualitatively confirmed tight junction integrity (ZO-1 protein expression) in cell layers. Confluent A549 cells exhibited honeycomb structures with ZO-1 staining. VWF and CD68 immunostaining served to validate the physiological conditions of the other two cell layers (EA.hy 926 and THP-1) in our co-culture model.

Monoculture models are very convenient for toxicity screening due to their simplicity. However, the lack of cell-cell interaction and cooperative function offered by different cell types may produce misleading results. Co-culture models have been developed to resolve this issue. The interactions between cell lines have been recognized in *in vitro* co-culture models, for example, communication has been observed in an epithelial-macrophage co-culture model exposed to ozone, and crosstalk was successfully initiated in an epithelial-endothelial co-culture model (Bauer et al., 2015; Blume et al., 2017). Cellular communications are usually quantified by the level of signaling mediators released. Under a certain stimulus, we expect to observe some elevation of signaling molecules for example, with ENM exposures we expect the co-culture model to express a higher level of cytokines/chemokines due to the presence of macrophages and endothelial cells to attract nearby immune cells. The toxicological response comparison between A549 cells and the co-culture model indicated potential cell-cell interaction in the co-culture model following ENM exposure. IL-8 is a chemokine secreted by epithelial cells, endothelial cells, macrophages, and monocytes upon inflammatory stimulus. It is also a potent chemokine for neutrophils to the lung (Bickel, 1993; Wickremasinghe et al., 1999; Standiford et al., 1990). In the co-culture model, we postulated increased IL-8 release with ENMs exposure due to enhanced cell-cell signaling. The response of co-cultures *vs.* A549 cells alone or macrophages alone produced much higher IL-8 release lending support for this postulate.

CuO ENMs have been studied extensively in our laboratory, in both *in vivo* and *in vitro* ALI systems. Jing et al. reported 15-fold and 30-fold higher IL-8 release compared with controls in A549 cells and human bronchial epithelial cells (HBECs), respectively, after 4 h of CuO ENMs exposure under ALI condition (Jing et al., 2015). The same trend was observed in our co-culture *vs.* monoculture results. A significantly higher IL-8 release was seen in the co-culture compared to the monoculture suggesting the co-culture model behaved more like the HBEC in terms of inflammation. Moreover, as postulated, we observed a significantly higher level of inflammatory response in the co-culture model than A549 cells for both materials. This phenomenon could be explained by pro-inflammatory functions of activated macrophages.

ROS production is another effect biomarker used in nanotoxicology studies. ENMs induce ROS production through different mechanisms. A variety of pathways have been proposed whereby a nanosized particle could induce oxidative stress. These include 1) NADPH oxidase mediated activation, 2) disruption of cytochrome P450, 3) mitochondrial electron transport chain interference, 4) macrophages releasing oxyradical in inflammatory state, and 5) conversion of oxygen metabolites into secondary ROS (Morishige et al., 2010; Yamakoshi et al., 2003; Sahu and Casciano, 2009; Oberdorster et al., 2005b). The determination of a specific ROS mechanism can be difficult and may result from diverse particle sizes and compositions, and even contamination. CuO ENMs have been found to induce ROS production both *in vitro* and *in vivo* (Jing et al., 2015; Kim et al., 2011; Boyles et al., 2016). Our ROS data support published results. The responses seen in the co-culture model *vs.* monoculture reflected the pattern observed in HBECs *vs.* A549 cells, confirming that the co-culture model had similarity in ROS production with the HBECs (Jing et al., 2015). Furthermore, when comparing the toxicity between materials, 15% Ag-SiO_2 ENMs induced a higher level of oxidative stress in the co-culture model than CuO ENMs. This difference may provide an indication that the toxicity of 15% Ag-SiO_2 may relate more strongly to ROS production.

5. Conclusions

We established and validated a three cell, co-culture model and used this model for toxicity assessment of citrate-capped Au, 15% Ag-SiO_2 and CuO ENMs. We further compared the biological responses with the monoculture models. Our results confirm that the complexity of the co-culture model enhanced measured responses over the monoculture system using the same ENMs. Our results further showed that the addition of endothelial cells (EA.hy 926) and differentiated macrophages (THP-1) to commonly used epithelial cell lines (A549) triggered some level of cooperation compared to A549 cells alone that led to a shift in biological responses toward enhanced ROS production and inflammation. Evidence about cellular interactions between cell lines was supported by comparing the level of IL-8 release after ENMs exposure in the co-culture model *versus* in A549 cells alone or macrophages alone. Despite enhanced responses in the co-culture ALI system, our results suggest that A549 cells alone provided a similar ranking of toxicity among the ENMs we tested.

Supplementary data to this article can be found online at https://doi.org/10.1016/j.impact.2020.100215.

Supplementary Material

Refer to Web version on PubMed Central for supplementary material.

Acknowledgement

Research reported in this publication was supported by the National Institute of Environmental Health Sciences of the U.S. National Institutes of Health under Award Number [NIH grant # U01ES027252] as part of the NHIR Consortium which focuses on comprehensive evaluation of interactions between ENMs and biological systems. The content is solely the responsibility of the authors and does not necessarily represent the official views of the National Institutes of Health.

The engineered nanomaterials used in the research presented in this publication have been procured/developed, characterized, and provided by the Engineered Nanomaterials Resource and Coordination Core established at Harvard T. H. Chan School of Public Health (NIH grant # U24ES026946) as part of the NHIR Consortium.

The research was conducted in laboratory facilities supported by the Environmental Health Sciences Research Center funded by NIH P30 ES005605.

References

Almofti MR, et al., 2003 Silver ion induces a cyclosporine a-insensitive permeability transition in rat liver mitochondria and release of apoptogenic cytochrome C. J. Biochem 134 (1), 43–49. [PubMed: 12944369]

AshaRani PV, et al., 2009 Cytotoxicity and genotoxicity of silver nanoparticles in human cells. ACS Nano 3 (2), 279–290. [PubMed: 19236062]

Bauer RN, et al., 2015 Interaction with epithelial cells modifies airway macrophage response to ozone. Am. J. Respir. Cell Mol. Biol 52 (3), 285–294. [PubMed: 25054807]

Beltran-Huarac J, et al., 2018 Development of reference metal and metal oxide engineered nanomaterials for nanotoxicology research using high throughput and precision flame spray synthesis approaches. NanoImpact 10, 26–37. [PubMed: 30035243]

Bickel M, 1993 The role of interleukin-8 in inflammation and mechanisms of regulation. J. Periodontol 64 (5 Suppl), 456–460. [PubMed: 8315568]

Blume C, et al., 2017 Cellular crosstalk between airway epithelial and endothelial cells regulates barrier functions during exposure to double-stranded RNA. Immunity Inflammation and Disease 5 (1), 45–56.

Bouis D, et al., 2001 Endothelium in vitro: a review of human vascular endothelial cell lines for blood vessel-related research. Angiogenesis 4 (2), 91–102. [PubMed: 11806248]

Boyles MSP, et al., 2016 Copper oxide nanoparticle toxicity profiling using untargeted metabolomics. Particle and Fibre Toxicology 13.

Brandenberger C, et al., 2010 Effects and uptake of gold nanoparticles deposited at the air-liquid interface of a human epithelial airway model. Toxicol. Appl. Pharmacol 242 (1), 56–65. [PubMed: 19796648]

Cho WS, et al., 2013 Comparative absorption, distribution, and excretion of titanium dioxide and zinc oxide nanoparticles after repeated oral administration. Part Fibre Toxicol 10, 9. [PubMed: 23531334]

Chuang CY, et al., 2011 Lipopolysaccharide induces apoptotic insults to human alveolar epithelial A549 cells through reactive oxygen species-mediated activation of an intrinsic mitochondrion-dependent pathway. Arch. Toxicol 85 (3), 209–218. [PubMed: 20848084]

Clement JL, Jarrett PS, 1994 Antibacterial silver. Met Based Drugs 1 (5–6), 467–482. [PubMed: 18476264]

Costantini LM, Gilberti RM, Knecht DA, 2011 The phagocytosis and toxicity of amorphous silica. PLoS One 6 (2), e14647. [PubMed: 21311600]

Dikalov SI, Harrison DG, 2014 Methods for detection of mitochondrial and cellular reactive oxygen species. Antioxid. Redox Signal 20 (2), 372–382. [PubMed: 22978713]

Dong J, et al., 2020 Synthesis of Precision Gold Nanoparticles Using Turkevich Method. KONA Powder and Particle Journal..

Edgell CJ, McDonald CC, Graham JB, 1983 Permanent cell line expressing human factor VIII-related antigen established by hybridization. Proc. Natl. Acad. Sci. U. S. A 80 (12), 3734–3737. [PubMed: 6407019]

Eweje F, et al., 2019 Quantifying the effects of engineered nanomaterials on endothelial cell architecture and vascular barrier integrity using a cell pair model. Nanoscale 11 (38), 17878–17893. [PubMed: 31553035]

Gibb S, 2008 Toxicity testing in the 21st century: a vision and a strategy. Reprod. Toxicol 25 (1), 136–138. [PubMed: 18093799]

Grigore ME, et al., Methods of Synthesis, Properties and Biomedical Applications of CuO Nanoparticles. Pharmaceuticals (Basel), 2016 9(4).

Hermanns MI, et al., 2004 Lung epithelial cell lines in coculture with human pulmonary microvascular endothelial cells: development of an alveolo-capillary barrier in vitro. Lab. Investig 84 (6), 736–752. [PubMed: 15077120]

Hussain SM, et al., 2005 In vitro toxicity of nanoparticles in BRL 3A rat liver cells. Toxicol. in Vitro 19 (7), 975–983. [PubMed: 16125895]

Jiang ZJ, Liu CY, Sun LW, 2005 Catalytic properties of silver nanoparticles supported on silica spheres. J. Phys. Chem. B 109 (5), 1730–1735. [PubMed: 16851151]

Jing X, et al., 2015 Toxicity of copper oxide nanoparticles in lung epithelial cells exposed at the air-liquid interface compared with in vivo assessment. Toxicol. in Vitro 29 (3), 502–511. [PubMed: 25575782]

Karlsson HL, et al., 2008 Copper oxide nanoparticles are highly toxic: a comparison between metal oxide nanoparticles and carbon nanotubes. Chem. Res. Toxicol 21 (9), 1726–1732. [PubMed: 18710264]

Katwal R, et al., 2015 Electrochemical synthesized copper oxide nanoparticles for enhanced photocatalytic and antimicrobial activity. J. Ind. Eng. Chem 31, 173–184.

Kessler R, 2011 Engineered nanoparticles in consumer products: understanding a new ingredient. Environ. Health Perspect 119 (3), a120–a125. [PubMed: 21356630]

Kiama SG, et al., 2001 Evaluation of phagocytic activity in human monocyte-derived dendritic cells. J Aerosol Med 14 (3), 289–299. [PubMed: 11693840]

Kim JS, et al., 2011 Effects of copper nanoparticle exposure on host defense in a murine pulmonary infection model. Part Fibre Toxicol 8, 29. [PubMed: 21943386]

Kim JS, et al., 2013 Validation of an in vitro exposure system for toxicity assessment of air-delivered nanomaterials. Toxicol. in Vitro 27 (1), 164–173. [PubMed: 22981796]

Klein SG, et al., 2013 An improved 3D tetraculture system mimicking the cellular organisation at the alveolar barrier to study the potential toxic effects of particles on the lung. Part Fibre Toxicol 10, 31. [PubMed: 23890538]

Lai X, et al., 2018 Intranasal delivery of copper oxide nanoparticles induces pulmonary toxicity and fibrosis in C57BL/6 mice. Sci. Rep. 8 (1), 4499. [PubMed: 29540716]

Modak SM, Fox CL Jr., 1973 Binding of silver sulfadiazine to the cellular components of Pseudomonas aeruginosa. Biochem. Pharmacol 22 (19), 2391–2404. [PubMed: 4200887]

Morishige T, et al., 2010 Titanium dioxide induces different levels of IL-1beta production dependent on its particle characteristics through caspase-1 activation mediated by reactive oxygen species and cathepsin B. Biochem. Biophys. Res. Commun 392 (2), 160–165. [PubMed: 20059972]

Murugadoss S, et al., 2017 Toxicology of silica nanoparticles: an update. Arch. Toxicol 91 (9), 2967–3010. [PubMed: 28573455]

Nabeshi H, et al., 2011 Amorphous nanosilica induce endocytosis-dependent ROS generation and DNA damage in human keratinocytes. Part Fibre Toxicol 8, 1. [PubMed: 21235812]

Oberdorster G, et al., 2005a Principles for characterizing the potential human health effects from exposure to nanomaterials: elements of a screening strategy. Part Fibre Toxicol 2, 8. [PubMed: 16209704]

Oberdorster G, Oberdorster E, Oberdorster J, 2005b Nanotoxicology: an emerging discipline evolving from studies of ultrafine particles. Environ. Health Perspect 113 (7), 823–839. [PubMed: 16002369]

Pettibone JM, et al., 2008 Inflammatory response of mice following inhalation exposure to iron and copper nanoparticles. Nanotoxicology 2 (4), 189–204.

Pradhan S, et al., 2016 Effect of sonication on particle dispersion, administered dose and metal release of non-functionalized, non-inert metal nanoparticles. J. Nanopart. Res 18 (9), 285. [PubMed: 27774036]

Ramnani SP, Biswal J, Sabharwal S, 2007 Synthesis of silver nanoparticles supported on silica aerogel using gamma radiolysis. Radiat. Phys. Chem 76 (8–9), 1290–1294.

Rothen-Rutishauser B, et al., 2007 Translocation of particles and inflammatory responses after exposure to fine particles and nanoparticles in an epithelial airway model. Part Fibre Toxicol 4, 9. [PubMed: 17894871]

Rothen-Rutishauser BM, Kiama SG, Gehr P, 2005 A three-dimensional cellular model of the human respiratory tract to study the interaction with particles. Am. J. Respir. Cell Mol. Biol 32 (4), 281–289. [PubMed: 15640437]

Russell AD, Hugo WB, 1994 Antimicrobial activity and action of silver. Prog. Med. Chem 31, 351–370. [PubMed: 8029478]

Sahu SC and Casciano DA, Nanotoxicity in vivo and in vitro models to health risks. 2009, John Wiley & Sons,: Chichester, West Sussex; Hoboken, NJ p. 1 online resource (636 p.).

Society AT, 1997 Adverse effects of crystalline silica exposure. American Thoracic Society Committee of the scientific assembly on environmental and occupational health. Am. J. Respir. Crit. Care Med 155 (2), 761–768. [PubMed: 9032226]

Srinivasan B, et al., 2015 TEER measurement techniques for in vitro barrier model systems. J Lab Autom 20 (2), 107–126. [PubMed: 25586998]

Standiford TJ, et al., 1990 Interleukin-8 gene expression by a pulmonary epithelial cell line. A model for cytokine networks in the lung. J. Clin. Invest 86 (6), 1945–1953. [PubMed: 2254454]

Wang Z, et al., 2012 CuO nanoparticle interaction with human epithelial cells: cellular uptake, location, export, and genotoxicity. Chem. Res. Toxicol 25 (7), 1512–1521. [PubMed: 22686560]

Wickremasinghe MI, Thomas LH, Friedland JS, 1999 Pulmonary epithelial cells are a source of IL-8 in the response to Mycobacterium tuberculosis: essential role of IL-1 from infected monocytes in a NF-kappa B-dependent network. J. Immunol 163 (7), 3936–3947. [PubMed: 10490995]

Yamakoshi Y, et al., 2003 Active oxygen species generated from photoexcited fullerene (C60) as potential medicines: O2-* versus 1O2. J. Am. Chem. Soc 125 (42), 12803–12809. [PubMed: 14558828]

Yeh YC, Creran B, Rotello VM, 2012 Gold nanoparticles: preparation, properties, and applications in bionanotechnology. Nanoscale 4 (6), 1871–1880. [PubMed: 22076024]

Yonker LM, et al., 2017 Development of a primary human co-culture model of inflamed airway mucosa. Sci. Rep 7 (1), 8182. [PubMed: 28811631]

Zimmerman JF, et al., 2019 Scatter enhanced phase contrast microscopy for discriminating mechanisms of active nanoparticle transport in living cells. Nano Lett. 19 (2), 793–804. [PubMed: 30616354]

Zucco F, et al., 2005 An inter-laboratory study to evaluate the effects of medium composition on the differentiation and barrier function of Caco-2 cell lines. Altern. Lab. Anim 33 (6), 603–618. [PubMed: 16372835]

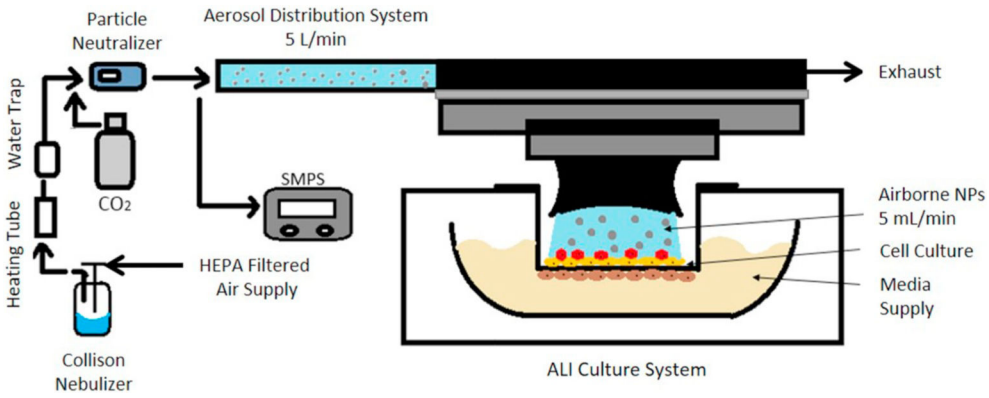

Fig. 1.

Simplified schematic of one of six cells of the air-liquid interface *in vitro* exposure system. It is composed of a NP aerosol generation system, an aerosol distribution unit, and an ALI culture system.

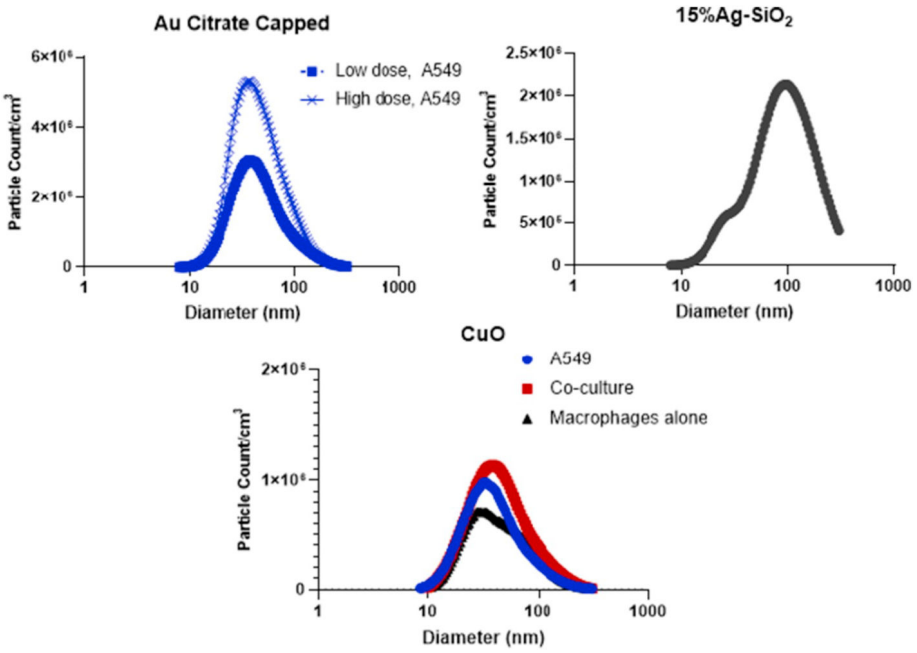

Fig. 2.

Particle counts and particle size distribution of low and high dose of Au citrate capped NPs, 15% Ag-SiO_2 and CuO NPs generated for the exposure of A549 cell, co-culture or macrophages only. Data for the 15% Ag-SiO_2 were obtained from separate experiments under the same nebulizer operating conditions. Measurements were performed by SMPS, geometric mean (GM) and geometric standard deviation (GSD) are reported in Table 2.

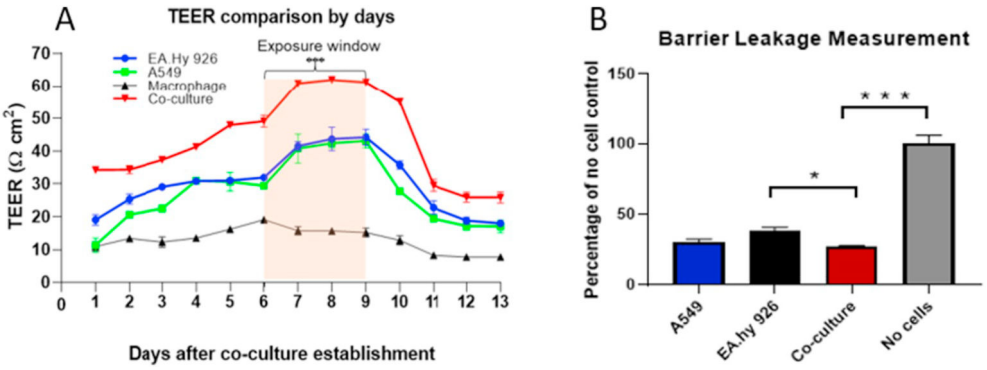

Fig. 3.

Transepithelial electrical resistance (Ohms/cm^2) was measured for the A549, EA.hy 926 cells and co-culture from day 1 to day 13 (A). All groups showed an increase in TEER up to day 6. From day 7 to day 9, the co-culture had stable resistance that was higher compared to the individual cell types. This increase was statistically significant ($P < 0.05$). Paracellular permeability was measured using sodium fluorescence tracer solution on day 9 in epithelial and endothelial cell lines as well as in co-culture (B). A group of no-cell controls was used to compare the amount of permeable fluorescence between each experimental group. Cell layers provided a significant level of blockage. The data were presented as mean ± S.D. * indicates $P < 0.05$; *** indicates $P < 0.001$.

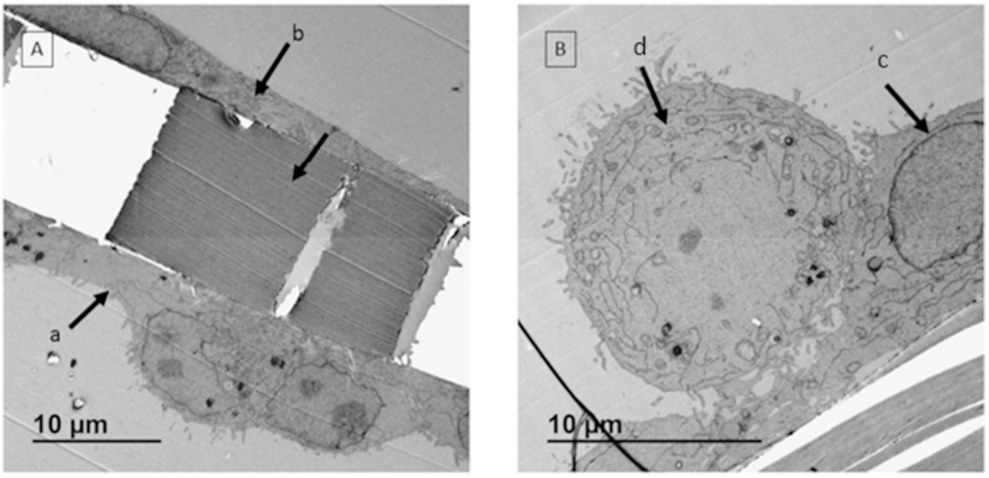

Fig. 4.

TEM images of co-culture model. A: Cell layers with different morphologies were observed on apical side (a) and basal side (b) of the transwell membrane. The space between a & b is the polyester membrane. B: On apical side, two cell layers with different morphologies were detected. The membrane was covered by epithelial cell layer (c) and macrophages were sitting on top of the membrane at an expected ratio (d).

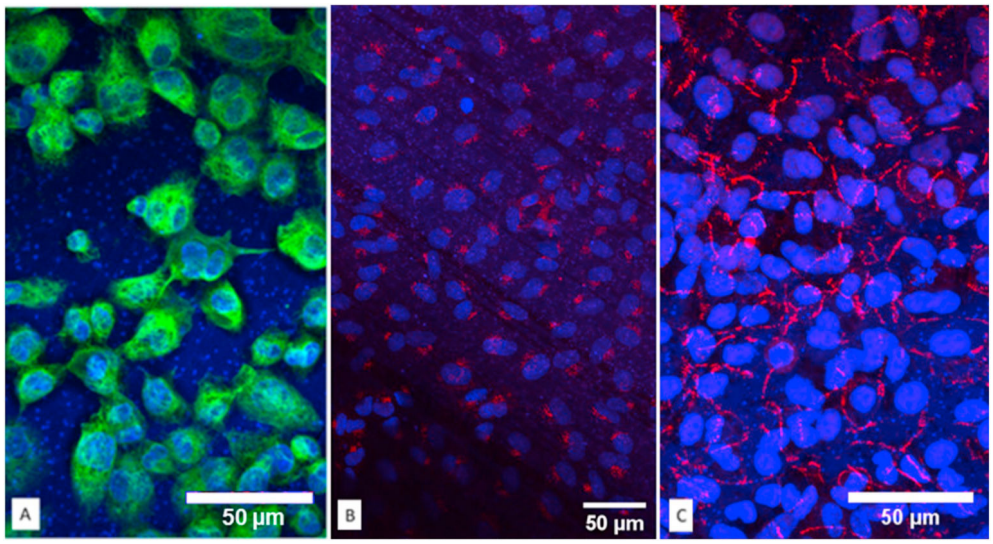

Fig. 5.

Immunofluorescent staining for key protein markers of the co-culture model were detected individually and combined. A: Macrophage CD68 protein signal was observed wrapping around nuclei in green. B: Specific endothelial protein VWF protein was detected only on the basal side of the polyester membranes. C: Tight junction protein ZO-1 lighted in far red as honeycomb shape in A549 cells. (For interpretation of the references to color in this figure legend, the reader is referred to the web version of this article.)

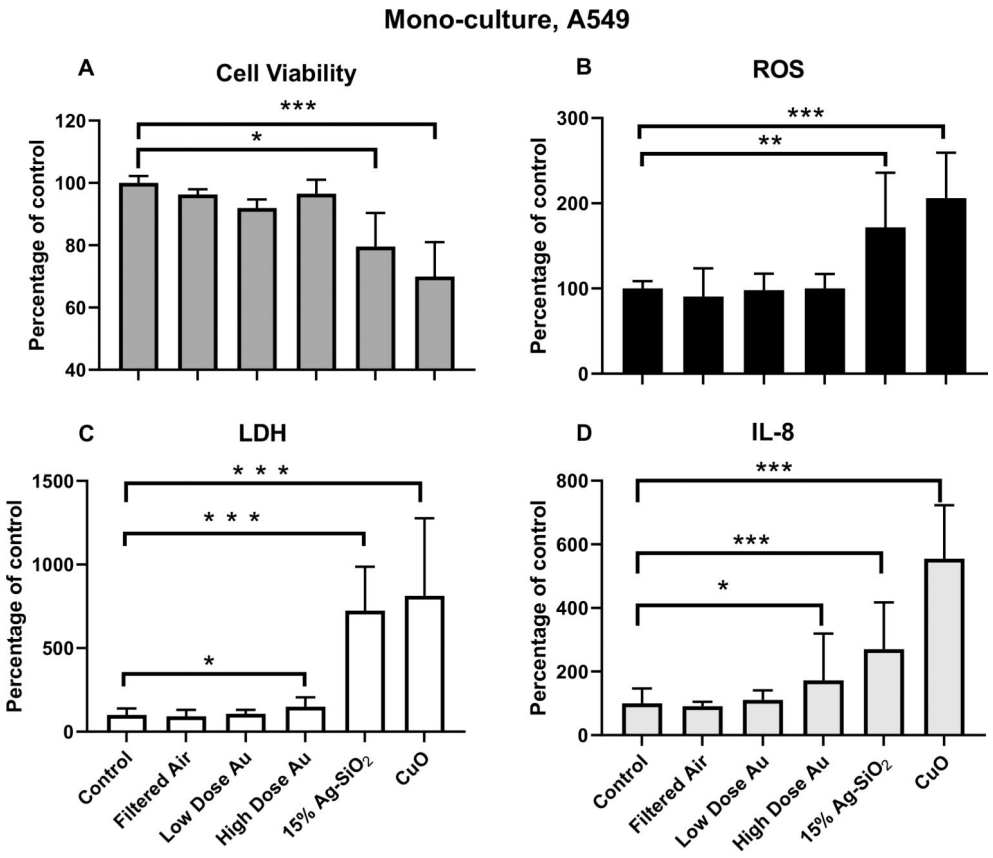

Fig. 6.

Toxicological responses of monoculture (A549 cells) after exposure to Au citrate-capped (low and high dose Au), 15% Ag-SiO_2, and CuO NPs expressed as percentage of controls (incubator controls). A. Cell viability B. ROS production C. LDH release D. Inflammatory cytokine IL-8. The data were presented as mean ± S.D. * indicates $P < 0.05$; ** indicates $P < 0.01$; *** indicates $P < 0.001$.

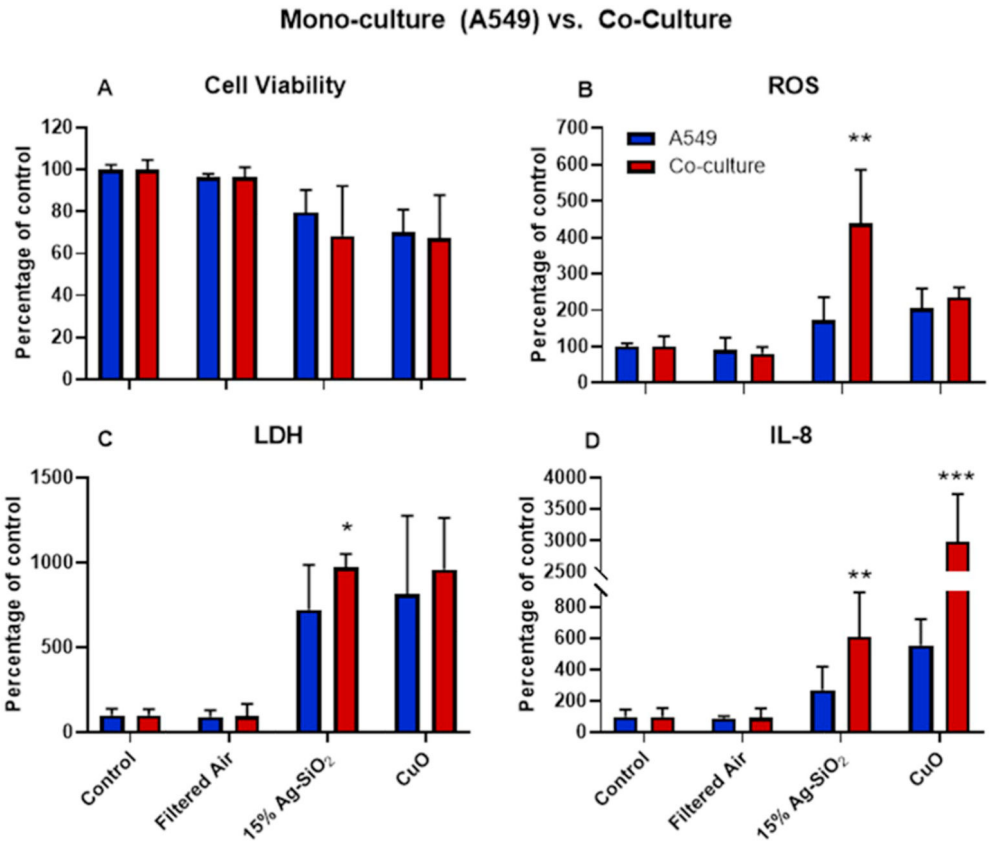

Fig. 7.

Cell viability (A), ROS generation (B), LDH release (D) and concentration of IL-8 (D) after exposure to 15% Ag-SiO_2 and CuO ENMs in monoculture (A549) and co-culture model. The data were presented as mean ± S.D. * indicates $P < 0.05$; ** indicates $P < 0.01$; *** indicates $P < 0.001$.

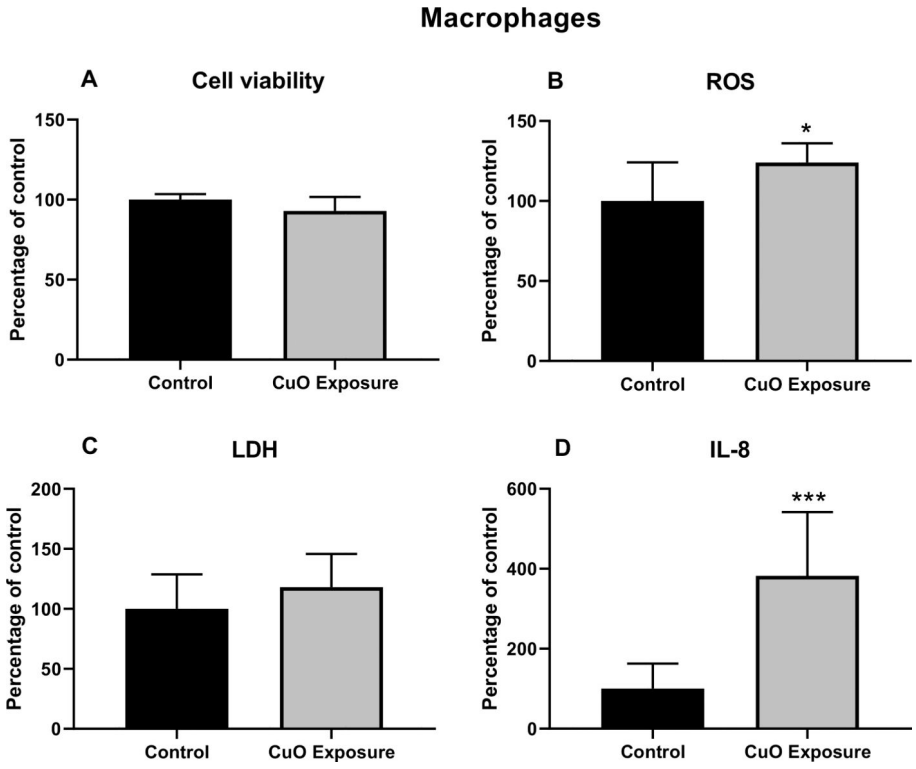

Fig. 8.

Toxicological responses of THP-1 differentiated macrophages after CuO NPs exposure under ALI condition. A. Cell viability B. ROS production C. Cytotoxicity measurement (LDH release) D. Inflammatory cytokine IL-8 level. The data were presented as mean ± S.D. * indicates $P < 0.05$; ** indicates $P < 0.01$; *** indicates $P < 0.001$.

Table 1

Morphological, structural, physical, chemical and biological properties of metal oxide ENMs studied.

Characterization parameters	Method	Citrate-capped Au (in suspension)	Silver supported on Silica (15% Ag-SiO_2)	Copper Oxide (CuO)
Synthesis method by ERCC/manufacturer		Hydrothermal	Flame Spray Pyrolysis	Sigma Aldrich
Primary particle size				
• Specific surface area (SSA) (m^2/g)	BET	–	333.1 ± 3.1	13.77 ± 0.68
• d_{BET} [b] (nm)	BET	–	6.4 (Ag), 6.1 (SiO_2)	70.9 ± 3.54
• d_{TEM} (nm)	TEM	18.36 ± 1.84 [e]	7.9 ± 4.3 (Ag)	50.24 ± 10.99
• d_{XRD} [a] (nm)	X-Ray Diffraction	–	5.8 (Ag)	25.8
Colloidal properties	Dynamic Light Scattering			
• d_{HYD} [c] (nm)	(DLS)	21.1 ± 0.3	135.2 ± 2.0	505.6 ± 51.1
• PDI		0.056 ± 0.011	0.287 ± 0.027	0.130 ± 0.018
• Zeta potential (mV)		−38.7 ± 2.9	22.2 ± 1.5	−19.0 ± 1.5
• pH		5.64	–	–
• Conductance (mS/cm)		0.229 ± 0.013	0.027 ± 0.0006	0.0184 ± 0.0002
Crystal structure	X-Ray Diffraction			
• Crystal system		–	Cubic, 87% (Ag)	Monoclinic Tenorite
• Crystallinity		Polycrystalline [d]	Amorphous, 0% (SiO_2)	Crystallinity: 73.1%
Shape factors				
• Aspect ratio ξ	TEM	1.12 ± 0.07	1.12 ± 0.14	1.35 ± 0.20
• Circularity ψ	TEM	0.96 ± 0.02	0.97 ± 0.09	0.93 ± 0.04
• Roundness ζ	TEM	0.90 ± 0.05	0.89 ± 0.11	0.76 ± 0.11
Porosity				
• Total pore volume (cm^3/g)	BET	–	0.46	1.87×10^{-4}
• Average pore size (nm)	BET	–	3.7	2.65
Raw density (g/cm^3)	Pycnometry [e]	19.3 (raw material density)	3.58 ± 0.25	6.1531 ± 0.0027
Particle purity	ICP-MS [f]	99.99 ± 0.31% (Au)	99.98 ± 0.03 (Ag)	98.21% ± 6.11% (Cu)
Endotoxin levels				

Characterization parameters	Method	Citrate-capped Au (in suspension)	Silver supported on Silica (15% Ag-SiO_2)	Copper Oxide (CuO)
• Concentration per mass of ENM (EU/mg)	Recombinant Factor	4.87	23.93	2.141
Sterility (bacteria/mg)	Suspension tested at 50 μg/mL	No growth	No growth	0
ERCC reference reporting on characterization data		Zimmerman et al. 2019, Dong et al., 2020	Beltran-Huarac et al., 2018	(Eweje et al., 2019)

NA: not applicable.

[a] d_{XRD}: particle diameter of ENMs determined from X-ray diffraction (XRD).

[b] d_{BET}: particle diameter of ENMs determined from Brunauer-Emmett teller (BET).

[c] d_{HYD}: hydrodynamic particle diameter.

[d] TEM Selected Area Electron Diffraction (SAED).

[e] Picnometry: the raw density of ENMs determined by nitrogen volume displacement (pycnometry).

[f] ICP-MS: inductively coupled plasma mass spectrometry.

Table 2

Size characteristics, exposure concentrations and aerosol size distributions of generated aerosols for in vitro studies.

Type of ENMs	Primary particle size[a]	Concentration in Collison nebulizer[c]	Exposure concentration, mg/m^3			Aerosol size distribution, GM nm, (GSD)[b]		
			A549	Co-culture	THP-1	A549	Co-culture	THP-1
Citrate- capped Au – low	18.36 ± 1.84	50 μg/mL[d]	1.58	–	–	43.9 (1.8)	–	–
Citrate- capped Au – high	18.36 ± 1.84	50 μg/mL[d]	2.48	–	–	43.7 (1.7)	–	–
15% Ag-SiO_2	7.9 ± 4.3 (Ag)	0.5 mg/mL	4.73	4.48	–	84.5 (1.9)	69.1 (2.0)	–
CuO	50.24 ± 10.99	1.5 mg/mL	3.62	3.93	1.81	35.4 (1.8)	42.9 (1.8)	42.4 (1.9)

[a] Primary particle size (geometric mean ± standard deviation) determined by transition electron microscopy provided by ERCC.

[b] GM: geometric mean mobility diameter (GM) with geometric standard deviation (GSD).

[c] All ENMs except Au were suspended in Optima ultrapure water.

[d] Au suspension was used as provided.

Table 3

Estimated deposited doses of ENMs used for ALI studies in mass per cell surface area. The nominal endotoxin exposure per transwell area is calculated based on the endotoxin concentration shown in Table 1.

Type of ENMs	ENM mass loading, ng/cm^2			Endotoxin loading, EU/cm^2		
	A549	Co-culture	THP-1	A549	Co-culture	THP-1
Citrate-capped Au – low	203	–	–	0.0010	–	–
Citrate-capped Au – high	319	–	–	0.0016	–	–
15% Ag-SiO_2	608	576	–	0.0145	0.0138	
CuO	465	505	233	0.0010	0.0011	